Impact of Back Surface Layers on the Performance of $Zn_xcd_{1-X}s/Cu_2SnS_3$ (CTS) Solar Cell

Md. Sharafat Hossain[1*], Rosni Roman Wahid[1], Md. Simul Hasan Talukder[1] and Md. Nasim Adnan[2]

[1]Department of Electrical and Electronic Engineering, Dhaka University of Engineering & Technology, Gazipur, Bangladesh
[2]Department of Computer Science and Engineering, Jashore University of Science & Technology, Bangladesh

ABSTRACT

The project focuses on the potentiality of CTS absorber layer in a $Zn_xCd_{1-x}S$/CTS solar cell, incorporating a back surface reflector (BSR), was explored through numerical simulations using the AMPS-1D (Analysis of Microelectronic and Photonic Structures) simulator. CTS has been identified as a favorable candidate among thin-film materials due to its optimal direct bandgap, high absorption coefficient, and suitable electronic properties. The primary objective of this study was to improve the cell output parameters of $Zn_xCd_{1-x}S$/CTS photovoltaic (PV) cell with micro-range absorber layers, aiming to significantly reduce production costs. The targeted $Zn_xCd_{1-x}S$/CTS PV cell shows 21.592% efficiency (V_{oc} = 1.049 V, J_{sc} = 27.841 mA/cm^2, FF = 0.805) with a 1 µm thick CTS absorber and without a back surface reflector (BSR). However, the proposed structures integrating with BSR configurations demonstrated promising results even with ultra-thin absorbers. Arsenic telluride (As_2Te_3) was selected as the BSR material for further investigation. The As_2Te_3-based BSR demonstrated a notable improvement in performance, achieving an efficacy of 23.433% (V_{oc} = 1.06 V, J_{sc} = 29.503 mA/cm^2, FF = 0.819) by an ultra-thin CTS absorber thickness of only 1 µm. It was also observed that increasing operating temperature significantly affects solar cell performance. Among the investigated configurations, the cell with BSR exhibited better thermal stability than the cell without BSR, with thermal tangent of -0.12%/^{0}K and -0.19%/^{0}K respectively. These simulation outcomes provide valuable insights into the feasible fabrication of cost-effective, non-toxic, highly efficient and thermal stable CTS-based cells.

1. INTRODUCTION

The second-generation thin-film material, Cu_2ZnSnS_4 (CZTS), has drawn substantial attention from contemporary researchers due to its favorable properties, making it a strong candidate as an absorber layer in thin-film solar cells. As a p-type quaternary semiconductor, CZTS exhibits excellent photovoltaic characteristics, including a high absorption coefficient exceeding 10^4 cm^{-1} and a direct bandgap ranging from approximately 1.4 to 1.56 eV [1–2], aligning well with the optimal range for single-junction solar cell applications. In recent years, CZTS has been widely explored as an eco-friendly and cost-effective alternative to conventional materials like CIGS and CdTe, as it consists of earth-abundant and non-toxic elements. However, one of the key challenges with CZTS is its narrow thermodynamic stability range, which often results in the formation of undesirable secondary phases such as binary compounds (CuS, SnS, SnS_2, ZnS) and ternary phases like Cu_2SnS_3 during its synthesis [3–6].

To address these limitations, researchers have been investigating other absorber materials that are both non-toxic and abundantly available. Among these, copper tin sulfide (Cu_2SnS_3 or CTS) has emerged as a promising alternative. Notably, CTS shares a similar crystal structure with CZTS and offers a direct bandgap in the range of 0.9 to 1.4 eV—close to the ideal value for photovoltaic applications. Additionally, CTS possesses a high absorption coefficient and p-type conductivity, making it a viable material for solar energy conversion [3, 6]. Interestingly, CTS can exhibit multiple crystal phases, such as cubic, monoclinic, tetragonal, triclinic, and hexagonal structures, where variations in cation and anion ordering influence its bandgap properties [7–12]. Several physical and chemical deposition techniques have been employed to fabricate CTS thin films, enhancing its applicability in photovoltaic technologies [6, 9, 11, 12–15]. Compared to these above-mentioned properties, CTS is one of the best choices of the current researcher as an absorber layer for the next generation thin film solar cells. Currently, the key objective of PV research and

*Corresponding author's email: sharafat@duet.ac.bd

development is to design and fabricate solar cells that are commercially feasible by meeting three central criteria: high efficiency, cost-effectiveness and stable operating capacity. Reducing the thickness of the CTS absorber layer can significantly decrease the amount of material required, thereby lowering fabrication costs. Minimizing the thickness of various layers in the overall solar cell structure not only cuts down on production expenses, energy consumption, and manufacturing time but also reduces the total material usage. These combined benefits contribute to making solar cells more affordable and accessible. In considering window material, conventional cadmium sulfide (CdS) presents several limitations when used as the window layer in CdTe/CTS-based thin-film solar cells. Among numerous limitations, the lattice mismatch between CdS and CdTe/CTS is approximately 10%, which introduces a high density of structural defects at their junction, adversely affecting cell performance. Due to these drawbacks, researchers have turned their attention to alternative window materials that offer higher bandgaps and better lattice compatibility. Some promising candidates include ZnS (bandgap ~3.70 eV), ZnSe (~2.69 eV), and the alloyed compound ZnxCd1-xS, which allows bandgap tuning between 2.42 and 3.70 eV depending on composition. Therefore, investigating the limits of CTS absorber layer thinning will be a central focus of this project. The theoretical and experimental efficiency of CTS thin film solar cell is increasing day by day in recent years [16-18]. Its efficiency remains far below the theoretical limit, and it has not yet been introduced commercially. Considering the potential for future commercialization of CTS technologies, attention has been directed towards developing a new device structure consisting of Glass/TCO/Front contact buffer layer/$Zn_xCd_{1-x}S$/CTS/Back Surface Reflector (BSR)/ suitable metal contact with promising window layer of $Zn_xCd_{1-x}S$. Efforts have been deliberately concentrated on optimizing the various layers of this proposed CTS solar cell to enhance its efficiency. Therefore, the aim of this project is to investigate a novel $Zn_xCd_{1-x}S/Cu_2SnS_3$ thin-film solar cell design, targeting improved conversion efficiency and reduced costs by minimizing the thickness of the material layers. Consequently, a novel device architecture featuring ultra-thin CTS layers with a back surface reflector (BSR) Glass/TCO/Zn_2SnO_4/$Zn_xCd_{1-x}S$/CTS/As_2Te_3/Al has been proposed, with various strategies being explored to enhance efficiency through improved cell designs. This work focuses on the analysis of Glass/TCO/Zn_2SnO_4/$Zn_xCd_{1-x}S$/CTS/As_2Te_3/Al using a computational modeling approach. Numerical simulation serves as a powerful tool for examining how variations in material characteristics impact device performance, enabling researchers to assess design feasibility, fine-tune structural parameters, and predict overall device behavior before physical fabrication. In this investigation, simulations were conducted using the AMPS-1D (Analysis of Microelectronic and Photonic Structures) [19] platform to evaluate how the thickness and charge carrier concentration of the monoclinic CTS absorber layer influence key performance metrics. In addition, the effect of varying the buffer layer thickness was examined to identify the most suitable option for forming an effective interface with the monoclinic CTS absorber and to determine its contribution to cell efficiency. Key output parameters, including open-circuit voltage (V_{oc}), short-circuit current density (J_{sc}), fill factor (FF), and power conversion efficiency (Eff), were systematically recorded and analyzed to assess the overall behavior of the proposed configurations.

2. METHODOLOGY

Before physically fabricating a solar cell, conducting a numerical investigation is a crucial step for evaluating how different design parameters influence device behavior and for identifying optimal configurations in a cost-effective manner. In the present study, simulations of $Zn_xCd_{1-x}S$/CTS thin-film solar cells were performed using the AMPS-1D software (Analysis of Microelectronic and Photonic Structures), a computational tool originally developed by Stephen Fonash and colleagues at Pennsylvania State University in 1999 [19]. This one-dimensional simulator is capable of modeling a wide variety of device structures, including heterojunctions, homojunctions, multijunction systems, and Schottky barrier-based solar cells. Users define the properties of each material layer in the simulated device, allowing for detailed customization of the model. AMPS-1D has been widely recognized and adopted across research groups due to its strong ability to replicate the physics and behavior of crystalline, polycrystalline, and amorphous photovoltaic devices. It utilizes finite difference methods along with the Newton-Raphson iterative approach to solve the coupled one-dimensional continuity and Poisson's equations for charge carriers. By inputting accurate material data, the software can compute essential device metrics such as open-circuit voltage (V_{oc}), short-circuit current density (J_{sc}), fill factor (FF), and efficiency (Eff), along with internal device characteristics including space charge region profiles, charge generation and recombination dynamics, and spectral response.

As shown in Fig. 1, the updated solar cell configuration includes an additional buffer layer—Zn_2SnO_4—inserted between the SnO_2 front contact and the $Zn_xCd_{1-x}S$ window layer. This modification aims to improve the effectiveness of the ultra-thin $Zn_xCd_{1-x}S$ layer. Additionally, although SnO_2 continues to serve as the transparent conductive oxide (TCO) at the front of the device, its thickness has been significantly reduced from the conventional 500 nm to 100 nm to help optimizing the cell's overall performance.

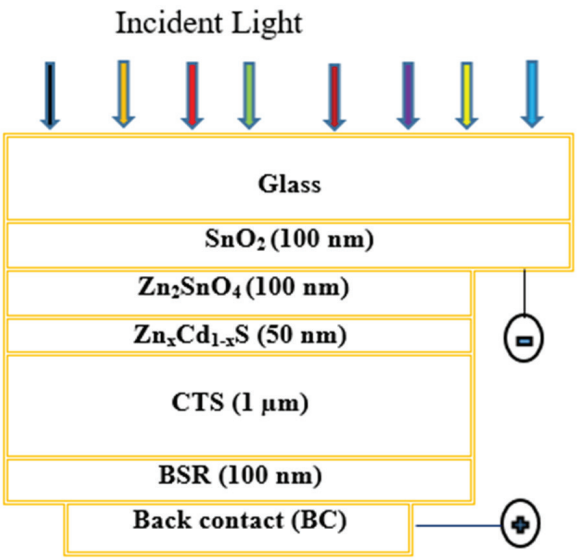

Fig. 1: Structures of the Proposed $Zn_xCd_{1-x}S$/CTS Cell for Enhanced Performance

To construct the front contact of the solar cell, SnO_2 is combined with a buffer layer of Zn_2SnO_4. The traditional CdS window layer has been replaced by $Zn_xCd_{1-x}S$, with the composition 'x' optimized for enhanced cell performance. The absorber layer is based on copper tin sulfide (CTS), selected due to its eco-friendly composition, economic viability, promising efficiency, and wide availability in nature. To mitigate performance limitations such as rollover effects, thermal instability, and minority carrier losses at the rear interface, specially chosen back surface reflector (BSR) layers [20, 21] have been incorporated into the redesigned ultra-thin $Zn_xCd_{1-x}S$/CTS configuration.

Instead of using costly gold (Au) as the rear electrode, aluminum (Al) has been adopted to maintain the necessary barrier height while significantly lowering production costs. Given the complexity of the simulation, which involves tuning over 50 individual parameters [22], many variables were fixed to realistic values to simplify the model. Identifying these constants was challenging because many are sensitive to fabrication techniques and can vary between batches. The values used for simulation inputs—sourced from published literature, theoretical analysis, or practical assumptions—are detailed in Tables I and II.

At this point in the study, it becomes critical to identify the most suitable value of 'x' in the $Zn_xCd_{1-x}S$ window layer using the input parameters provided in Table II. The simulation process involved systematically modifying the thicknesses of different layers: the CTS absorber thickness was explored in the range of 100 nm to 3 µm; the $Zn_xCd_{1-x}S$ window layer varied between 25 nm and 200 nm; the Zn_2SnO_4 buffer layer was adjusted from 25 nm up to 500 nm; and the SnO_2 front contact layer was tuned within the same thickness range. All remaining parameters were kept fixed, as outlined in Table I.

The scope of analysis also extended to the effects of doping concentration in the absorber layer, variations in minority carrier lifetime, bandgap shifts within the absorber, and performance response to changing operational temperatures. There remains strong potential for improving $Zn_xCd_{1-x}S$/CTS solar cell performance by optimizing critical parameters such as open-circuit voltage (Voc), short-circuit current (Jsc), and fill factor (FF). This can be accomplished through refinement of the front contact buffer layers (Zn_2SnO_4) and the back surface reflector (BSR) layer (As_2Te_3). All simulations were carried out using the AMPS-1D modeling platform. Detailed interpretation of these results follows in the next section.

Table I: Different Layers' Properties used for Numerical Modelling

Parameter	n-SnO_2	n-ZnO	p-CTS	BSR (As_2Te_3)	Comments and references
W (µm)	0.025-0.5	0.025-0.5	0.1-3.0	0.1	Theory & estimations
$\varepsilon/\varepsilon_0$	9.0	9.0	10	20	[23], [3], [16], [24]
μ_e (cm^2/Vs)	100	100/32	100	500	[23], [3], [16], [24]
μ_p (cm^2/Vs)	25	25/03	25	210	[23], [3], [16], [24]
n,p (cm^{-3})	1×10^{17}	1×10^{19}	1×10^{14}~1×10^{16}	6.8×10^{19}	[23], [3], [16], [24]
E_g (eV)	3.60	3.0/3.35	0.9-1.4	0.6	[23], [3], [16], [24]
N_c (cm^{-3})	2.2×10^{18}	2.2×10^{18}	2.2×10^{18}	1×10^{16}	[23], [3], [16], [24]
N_v (cm^{-3})	1.8×10^{19}	1.8×10^{19}	1.8×10^{19}	1×10^{17}	[23], [3], [16], [24]
χ (eV)	4.5	4.35/4.50	4.77	4.0	[23], [3], [16], [24]

Table II: Material Properties [24-25] of n-$Zn_xCd_{1-x}S$ used for Simulation

Parameter	x = 0.05	x = 0.08	x = 0.1	x = 0.2	x = 0.3	x = 0.5	x = 0.6	x = 0.8
W (μm)	0.1	0.1	0.1	0.1	0.1	0.1	0.1	0.1
$\varepsilon/\varepsilon_0$	9.3	9.3	9.3	9.3	9.3	9.3	9.3	9.3
$\mu_e(cm^2/Vs)$	100	100	95	85	75	70	65	60
$\mu_p(cm^2/Vs)$	40	40	35	30	25	20	15	10
n,p (cm^{-3})	3.0×10^{16}	2.5×10^{16}	2.5×10^{16}	1.7×10^{16}	1.6×10^{16}	4.1×10^{15}	2.5×10^{15}	1.7×10^{15}
E_g (eV)	2.48	2.50	2.55	2.58	2.64	2.70	3.07	3.33
N_c (cm^{-3})	2.1×10^{18}	2.1×10^{18}	2.1×10^{18}	2.1×10^{18}	2.1×10^{18}	2.1×10^{18}	2.1×10^{18}	2.1×10^{18}
N_v (cm^{-3})	1.7×10^{19}	1.7×10^{19}	1.7×10^{19}	1.7×10^{19}	1.7×10^{19}	1.7×10^{19}	1.7×10^{19}	1.7×10^{19}
χ (eV)	4.47	4.46	4.44	4.38	4.32	4.26	4.14	4.02

3. RESULTS AND DISCUSSIONS

To develop a high-efficiency solar cell, a $Zn_xCd_{1-x}S$ /CTS configuration was adopted using a superstrate design. This approach emphasized the strategic arrangement and optimization of individual layers, including reduced thicknesses and the integration of experimentally validated doping concentrations. Improvements were also made to the front and rear contact interfaces. In this updated structure, commercially available SnO_2 was chosen as the front contact material, with its thickness reduced from 500 nm to 100 nm to enhance overall performance of the solar cell. The window layer consisted of $Zn_xCd_{1-x}S$, while CTS functioned as the primary absorber layer. To limit the forward leakage current often associated with ultra-thin $Zn_xCd_{1-x}S$ layers, the window thickness was constrained to 50 nm. A Zn_2SnO_4 buffer layer was introduced between SnO_2 and $Zn_xCd_{1-x}S$, serving the dual purpose of charge carrier management and acting as a back surface layer (BSR). Further tuning of the window composition revealed that a 30% zinc concentration yielded optimal performance improvements.

3.1 Front Contact's Buffer Layer Selection

To enhance the efficiency of $Zn_xCd_{1-x}S$ /CTS thin-film solar cells, the window layer thickness was reduced to minimize parasitic absorption. However, excessive thinning can cause forward leakage due to pinhole formation—though less severe than in CdS-based layers. To counter this, a high-resistivity Zn_2SnO_4 buffer was added between SnO_2 and $Zn_xCd_{1-x}S$. This design improves structural quality by promoting larger grain growth and maintains good lateral current collection via the SnO_2 front contact. Simulations using AMPS-1D, with a 1 μm CTS absorber, 50 nm $Zn_xCd_{1-x}S$ window, and 100 nm SnO_2 front layer, showed that both doped and undoped Zn_2SnO_4 buffers yield comparable performance. The resulting J–V characteristics are shown in Fig. 2.

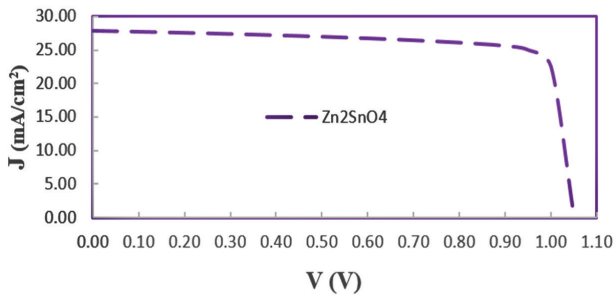

Fig. 2: Influence of Zn_2SnO_4 on J-V Curve of $Zn_xCd_{1-x}S$/CTS Solar Cell

Additional simulations were conducted to investigate the influence of buffer layer thickness on the overall performance of the solar cell. The results indicated that the primary performance indicators remained relatively consistent when the Zn_2SnO_4 buffer thickness varied between 25 nm and 500 nm. Moreover, the spectral response (SR) exhibited minimal variation across this range, suggesting that even a relatively thin buffer layer is sufficient to maintain optimal device operation. Considering practical aspects of fabrication, a buffer thickness of 100 nm was chosen as the standard for all devices in this study, as it offers a favorable compromise between efficiency and ease of manufacturability.

3.2 Optimization of Zn, Cd ratio in $Zn_xCd_{1-x}S$ Window Layer

In the proposed enhanced $Zn_xCd_{1-x}S$/CTS solar cell design, an additional Zn_2SnO_4 layer is introduced between the SnO_2 and $Zn_xCd_{1-x}S$ layers. To analyze the effect of varying zinc concentration (x) on the device's conversion efficiency, numerical simulations were performed for values of x ranging from 0 to 1. The simulations utilized material and device parameters detailed in Table II, based on data reported in references [24-25]. The modeled structure included a 1 μm thick CTS absorber layer, a 100 nm Zn_2SnO_4 buffer layer, and an aluminum (Al) rear metal contact.

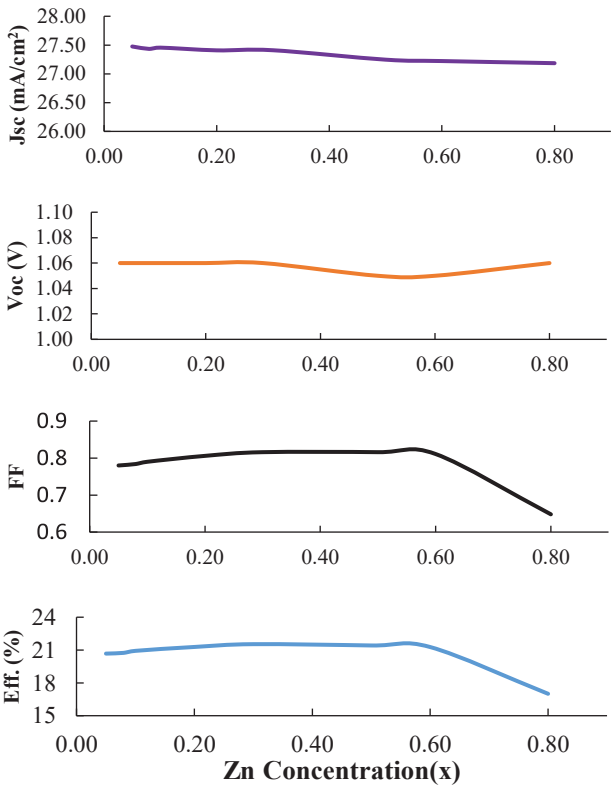

Fig. 3: Impact of Zn Concentration on $Zn_xCd_{1-x}S$/CTS Cell Output Parameters

As illustrated in Fig. 3, the solar cell demonstrated improved performance metrics—namely, higher conversion efficiency, open-circuit voltage (V_{oc}), and fill factor (FF)—at lower zinc concentrations ($x \leq 0.3$). The short-circuit current density (Jsc) remained relatively stable up to x = 0.3 but showed a gradual decline as the zinc content increased beyond this point. Specifically, the simulation yielded efficiencies of 20.672% (V_{oc} = 1.06 V, J_{sc} = 27.475 mA/cm², FF = 0.780) for x = 0.05 and 21.537% (V_{oc} = 1.06 V, J_{sc} = 27.410 mA/cm², FF = 0.816) for x = 0.3. Furthermore, the resistivity of the $Zn_xCd_{1-x}S$ layer was observed to rise substantially, from 1 Ω·cm at x = 0 to approximately 10^{10} Ω·cm at x = 1 [26]. Considering the combined impact of fabrication feasibility, electrical resistivity, and simulation results, a zinc concentration of x = 0.3 was identified as optimal for the window layer. Accordingly, all subsequent device configurations presented in the following section adopt $Zn_xCd_{1-x}S$ with x = 0.3.

3.3 Effect of $Zn_xCd_{1-x}S$ Window Layer's Thickness

This study also examined the impact of the $Zn_xCd_{1-x}S$ (x=0.3) window layer thickness on the overall performance of the solar cell. To assess this, simulations were conducted with the window layer thickness varied between 25 nm and 200 nm. The device architecture for the simulations included a 1 µm CTS absorber layer, a 100 nm Zn_2SnO_4 buffer layer, a 100 nm SnO_2 front contact, and an aluminum (Al) rear electrode. The results of these simulations are presented in Fig. 4. As shown in Fig. 4, increasing the thickness of the $Zn_xCd_{1-x}S$ (x = 0.3) window layer led to a clear decrease in short-circuit current density (Jsc) and overall conversion efficiency, while the fill factor (FF) remained nearly constant. Interestingly, the open-circuit voltage (Voc) initially increased with greater thickness but began to decline after reaching a certain threshold. This trend is attributed to the fact that a thicker window layer absorbs more incident photons before they can reach the CTS absorber, thereby reducing the generated photocurrent. In contrast, thinner $Zn_xCd_{1-x}S$ layers improve efficiency mainly due to enhanced Jsc. However, extremely thin layers can develop pinholes, potentially resulting in forward leakage currents. To counteract this, a high-resistivity Zn_2SnO_4 buffer was included between the SnO_2 and $Zn_xCd_{1-x}S$ layers. Balancing fabrication feasibility with device performance, a window layer thickness of 50 nm for $Zn_xCd_{1-x}S$ (x = 0.3) was determined to be optimal, yielding a conversion efficiency of 21.592%, with V_{oc} = 1.049 V, J_{sc} = 27.841 mA/cm², and FF = 0.805.

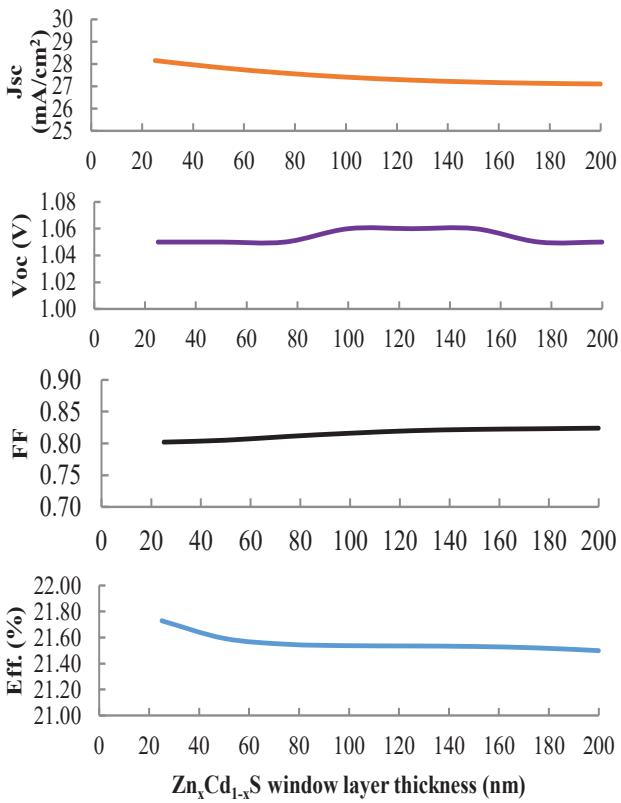

Fig. 4: Effect of Thicknesses Variation of Window Layer on $Zn_xCd_{1-x}S$/CTS Cell Parameter

3.4 Thickness Variation of CTS Absorber Layer

To evaluate material savings and cost efficiency, additional simulations were conducted by varying the CTS absorber thickness from 0.1 µm to 3 µm in the $Zn_xCd_{1-x}S$ /CTS (x = 0.3) solar cell. The configuration included a 50 nm $Zn_xCd_{1-x}S$ window layer, 100 nm Zn_2SnO_4 buffer, 100 nm SnO_2 front contact, and an aluminum (Al) back contact. As shown in Fig. 5, device performance remains stable for CTS thicknesses above 1.5 µm. Reducing the thickness led to a gradual drop in Jsc and efficiency, while V_{oc} and FF were largely unchanged until the thickness fell below 0.5 µm—beyond which all performance metrics sharply declines, likely due to limited minority carrier diffusion. These results indicate that CTS layers thinner than 0.5 µm are unsuitable for this configuration. However, a 1 µm CTS layer achieved a strong performance, with an efficiency of 21.592%, with V_{oc} = 1.049 V, J_{sc} = 27.841 mA/cm², and FF = 0.805, only 0.930% lower than that of the 3 µm design (22.522%), while using significantly less material. Thus, a 1 µm CTS absorber is considered optimal for further simulations, offering a practical balance between efficiency, material usage, and deposition time.

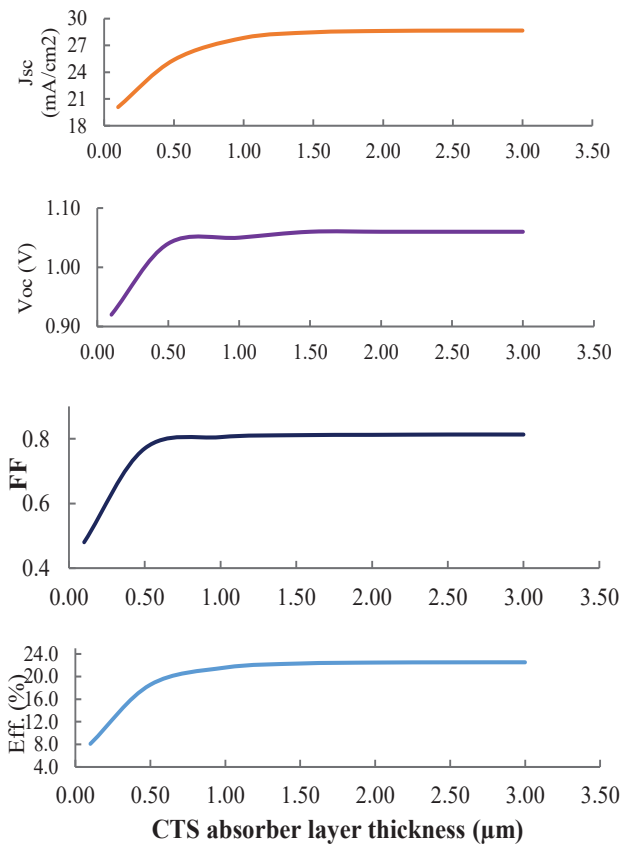

Fig. 5: CTS Thickness Variation Influences the Performance of $Zn_xCd_{1-x}S$/CTS Cell

1.1 Impact of Absorber Layer Doping Concentration

The doping concentration in the absorber layer significantly influences solar cell performance. In this part of the study, simulations were performed using a fixed device structure comprising a 1 µm CTS absorber, 50 nm $Zn_xCd_{1-x}S$ (x = 0.3) window layer, 100 nm Zn_2SnO_4 buffer, 100 nm SnO_2 front contact, and aluminum (Al) back contact.

To explore the effect of doping on device performance, the acceptor concentration in the p-type CTS absorber was varied from 4×10^{10} cm^{-3} to 4×10^{16} cm^{-3}. The resulting performance characteristics of the $Zn_xCd_{1-x}S$ /CTS (x = 0.3) thin-film solar cell are shown in Fig. 6. As depicted in Fig. 6, the solar cell's performance remains stable when the doping concentration ranged from 4×10^{10} cm^{-3} to 4×10^{13} cm^{-3}. However, beyond 4×10^{13} cm^{-3}, most output parameters improved, except for the short-circuit current density (Jsc), which gradually decreased. This reduction in Jsc is attributed to a decreasing depletion width in the p-type CTS absorber with increasing doping levels. In contrast, both the open-circuit voltage (Voc) and fill factor (FF) increased due to a rise in the built-in voltage. The solar cell achieved peak conversion efficiency of 21.592% at a doping concentration of 4×10^{16} cm^{-3}. This concentration is therefore selected as the standard for further simulations and analysis.

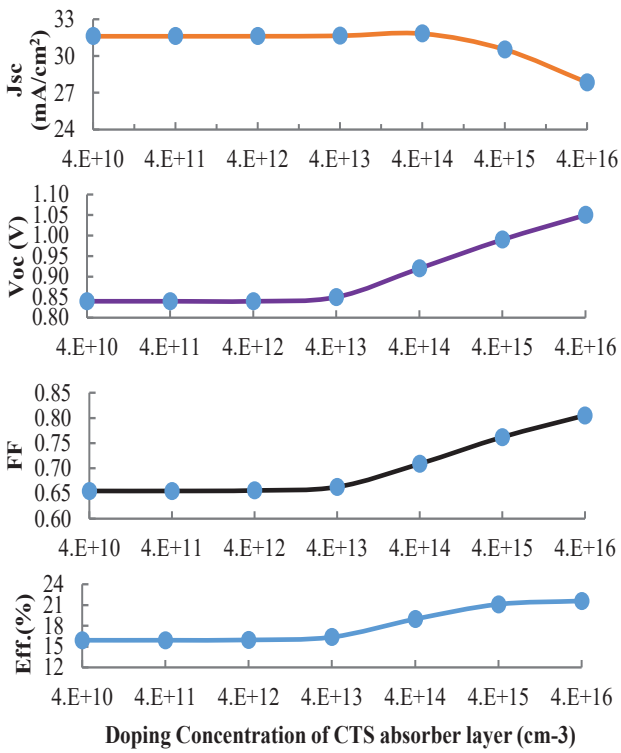

Fig. 6: Effect of the CTS Doping Concentration on Cell Output Parameters

3.6 Effect of Operating Temperature without BSR

Operating temperature plays a crucial role in solar cell performance. While the ideal operating temperature is around 298 K (room temperature), solar panels are often exposed to higher temperatures in outdoor conditions due to direct sunlight. Elevated temperatures can affect key material properties such as the effective density of states, absorption coefficients, carrier mobility, band gaps, and carrier concentrations. To evaluate the thermal stability of the proposed solar cell design (without a back surface reflector, BSR), the impact of increased operating temperatures was examined. In this simulation, the cell temperature was varied between 298 K and 400 K to assess the resulting performance changes. The outcomes are shown in Fig. 7.

As shown in Fig. 7, the normalized efficiency of the solar cell without a back surface reflector (BSR) layer decreases linearly with rising operating temperature, exhibiting thermal tangent of -0.19%/K. This low TC indicates that the cell maintains strong thermal stability and experiences minimal performance degradation under higher temperature conditions.

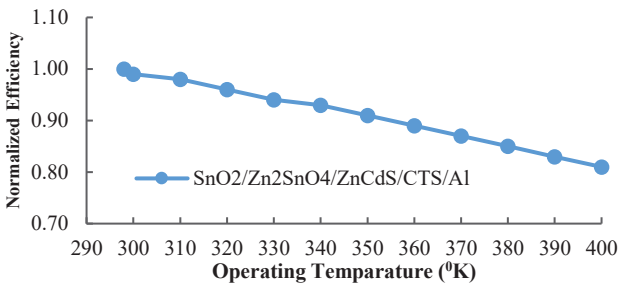

Fig. 7: Effect of Operating Temperature on Normalized Efficiency without BSR

3.7 Effect of Back Surface Reflector (BSR) on the $Zn_xCd_{1-x}S$/CTS Solar Cell Structure

To assess the impact of electron-hole reflectors on ultra-thin cell performance, this study explores a CTS solar cell with a carefully chosen BSR layer. The numerically modeled ultra-thin cell, consisting of a 1 µm CTS absorber layer, 50 nm $Zn_xCd_{1-x}S$ (x = 0.3) window layer, 100 nm Zn_2SnO_4 buffer, 100 nm SnO_2 front contact, and Al back contact, demonstrates strong performance with a conversion efficiency of 21.592%, J_{sc} of 27.841 mA/cm², V_{oc} of 1.049 V, and FF of 0.805%. The carrier lifetime in this model is 1.6 ns, with a hole concentration of 4×10^{16} cm^{-3}. The corresponding J–V curve for this ultra-thin device is shown in Fig. 8.

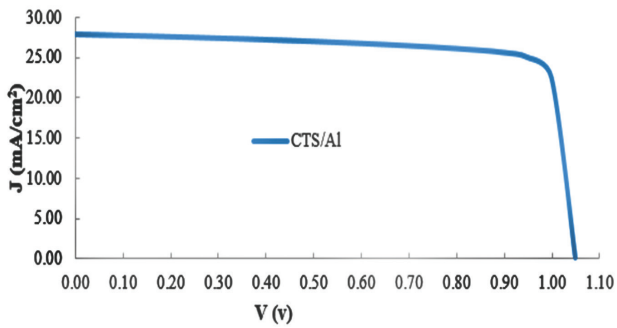

Fig. 8: J-V Curve of the Modified Cell Structure without any BSR Layer

This section investigates the potential of Arsenic Telluride (As_2Te_3) as a back surface reflector (BSR) material to reduce recombination losses in ultra-thin CTS solar cells. As_2Te_3, a p-type semiconductor with a low optical band gap, reflects minority carriers (electrons) back toward the front contact and helps holes move toward the back contact, minimizing rear interface recombination. The feasibility of using As_2Te_3 in thin-film solar cells was first proposed by M. A. A. Noman et al. [20].

A numerical simulation was conducted to evaluate the impact of the As_2Te_3 BSR on the performance of the ultra-thin $Zn_xCd_{1-x}S$ /CTS cell. The cell structure remained unchanged except for the addition of a 100 nm As_2Te_3 BSR layer at the back contact. The full structure includes a 1 µm CTS absorber, 50 nm $Zn_xCd_{1-x}S$ (x = 0.3) window layer, 100 nm Zn_2SnO_4 buffer layer, 100 nm SnO_2 front contact, and a 100 nm As_2Te_3 BSR layer. The results, presented in Table III, show that integrating the BSR layer significantly improves the efficiency of the solar cell. Without the BSR, the proposed ultra-thin $Zn_xCd_{1-x}S$/ CTS cell achieves a conversion efficiency of 21.592%. With the addition of the 100 nm As_2Te_3 BSR layer, the efficiency increases to 23.433%. This performance gain is attributed to improvements in short-circuit current density (J_{sc}), open-circuit voltage (V_{oc}), and fill factor (FF), highlighting the positive effect of the BSR. The J–V characteristics for both versions of the solar cell are shown in Fig. 9, confirming the enhancement in performance.

As shown in Fig. 9, the solar cell with the As_2Te_3 BSR layer exhibits improved open-circuit voltage (V_{oc}), short-circuit current density (J_{sc}), and fill factor (FF) compared to the cell without a BSR. These improvements are attributed to reduced back surface recombination and enhanced back contact quality with the p-type CTS absorber layer. As a result, the conversion efficiency of the cell with the As_2Te_3 BSR is significantly higher than that of the cell without the BSR layer.

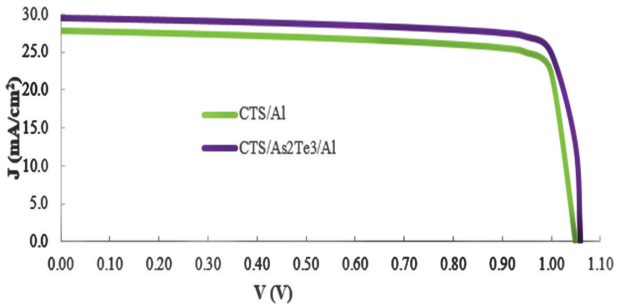

Fig. 9: Effect of BSR on the J-V Curves of the $Zn_xCd_{1-x}S$/CTS Solar Cell

3.8 Effect of Operating Temperature with BSR

Before drawing final conclusions regarding the performance of the As_2Te_3 BSR, it is essential to evaluate the thermal stability of the proposed structure under elevated operating temperatures.

As shown in Fig. 10, the efficiency of the cell without a BSR layer decreases linearly with rising temperature, exhibiting a thermal tangent of –0.19%/K. In contrast, the cell with the As_2Te_3 BSR layer shows significantly improved thermal stability, with efficiency remaining stable from 298 K to 330 K and a reduced thermal tangent of –0.12%/K beyond 330 K. The thermal tangent of |–0.19| %/K is significantly greater than the thermal tangent of |–0.12| %/K. This indicates better performance retention at higher temperatures, highlighting the effectiveness of As_2Te_3 as a BSR in ultra-thin CTS solar cells.

Table III: The Output Parameters of Modified Cells without and with As2Te3 BSR

Cells Structures	Output parameters			
	V_{oc} (V)	J_{sc} (mA/cm²)	FF	Eff. (%)
Glass/SnO_2/Zn_2SnO_4/$Zn_xCd_{1-x}S$/CTS/Al (x = 0.3)	1.05	27.841	0.805	21.592
Glass/SnO_2/Zn_2SnO_4/$Zn_xCd_{1-x}S$ /CTS/ As_2Te_3/Al (x = 0.3)	1.06	29.503	0.819	23.433

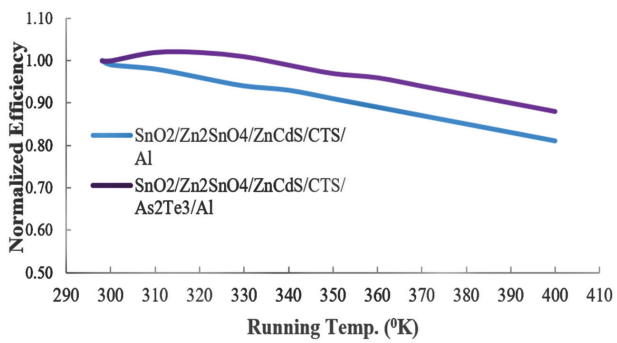

Fig. 10: Effect of Operating Temperature on Normalized Efficiency without and with As_2Te_3 BSR

3.9 Comparative Analysis with Other Published Works

This study aimed to evaluate the simulation results against previously published works. The proposed cell structure—glass/SnO_2/Zn_2SnO_4/$Zn_xCd_{1-x}S$/CTS/As_2Te_3/Al achieved a peak efficiency of 23.433%, with V_{oc} = 1.06 v, J_{sc} = 29.503 mA/cm², and FF = 0.819 for x=0.3. These results show significantly higher V_{oc} and J_{sc}, though the ff is slightly lower compared to other studies (table IV). The higher V_{oc} is likely due to improved lattice matching and reduced defect states at the p-CTS/n-$Zn_xCd_{1-x}S$ (x = 0.3) junction. Based on these findings, doping the window layer with indium (in) could further reduce resistivity and enhance performance. This structure represents a promising candidate for high-efficiency $Zn_xCd_{1-x}S$/CTS solar cells.

Table IV: Comparison between Proposed and other Published Works

Structures	Output parameters				Ref.
	V_{oc}(V)	FF	J_{sc} (mA/cm²)	Eff. (%)	
Mo/$CuSbS_2$/ CdS/ZnO/ ZnO:Al/Contact	0.65	0.6652	24.46	10.71	[21]
FTO/CTS/ZnS/ Ag	0.4252	0.7818	24.82	8.25	[3]
p-CTS/Zn(O, S)/n-ZnO/Al	0.3802	0.7445	48.33	13.65	[16]
Glass/SnO_2/ Zn_2SnO_4/ $Zn_xCd_{1x}S$/CTS/ As_2Te_3/Al (x=0.3)	23.433	0.819	29.503	1.06	Proposed

4. CONCLUSION

This research aimed to design and simulated an ultra-thin CTS solar cell using a Zn_xCd_{1-x}Swindow layer, replacing the conventional CdS/CTS setup, to enhance conversion efficiency via a suitable back surface reflector (BSR). Simulations were conducted using the AMPS-1D tool, with a proposed structure of Glass/SnO_2/Zn_2SnO_4/$Zn_xCd_{1-x}S$/CTS/AS_2Te_3/Al.

Efficiency enhancement was achieved by optimizing the window layer thickness to 50 nm and adding a 100 nm Zn_2SnO_4 buffer layer, improving spectral response—especially in the blue range, Zn_2SnO_4 delivered comparable performance. The optimal window composition was found at x = 0.3 in $Zn_xCd_{1-x}S$. Additionally, CTS absorber

thickness was minimized to 1 μm without significant loss in efficiency. Arsenic telluride (As_2Te_3) was introduced as a BSR due to its carrier reflection capabilities. While it had little effect on thicker absorbers, it significantly improved performance in thin-cell configurations. Incorporating a 100 nm As_2Te_3 BSR with a 1 μm CTS layer resulted in a peak efficiency of 23.433% (V_{oc} = 1.06 V, J_{sc} = 29.503 mA/cm², FF = 0.819).

The thermal performance of the optimized structure ($SnO_2/Zn_2SnO_4/Zn_xCd_{1-x}S$/CTS/$As_2Te_3$/Al, x = 0.3) was also assessed, showing a low thermal tangent of –0.12%/K, indicating good thermal stability. Overall, the proposed structure is suitable for practical fabrication, offering a non-toxic, efficient, and cost-effective alternative for CTS-based solar cells.

ACKNOWLEDGEMENT

The authors would like to acknowledge and appreciate UGC and DUET for the financial support to run the project work.

REFERENCES

[1] K. Devendra, D. Shah, S. Kumar, N. Bhattarai, D. Adhikari, K. B. Khattri, M. S. Akhtar, A. Umar, A. Ibrahim, M. A. M. Alhamami, S. Baskoutas, O. Yang Less, "Enhanced solar cell efficiency: Copper zinc tin sulfide absorber thickness and defect density analysis," Journal of Materials Science, Vol. 34, No. 24, p. 11125, 2023.

[2] H. Wei, W. Guo, Y. Sun, Z. Yang, Y. Zhang, "Hot-injection synthesis and characterization of quaternary $Cu_2ZnSnSe_4$ nanocrystals," Materials Letters, Vol. 64, pp. 1424–1426, 2010.

[3] S. Rahaman, M. K. Singha, P. Sarkar, M. A. Sunil, K. Ghosh, "Optimization of CTS thin film solar cell: A numerical investigation based on USP deposited thin films," Physica B: Condensed Matter, Vol. 698, p. 416751, 2025.

[4] S. Chen, X. G. Gong, A. Walsh, and S. H. Wei, "Defect physics of the kesterite thin-film solar cell absorber Cu_2ZnSnS_4," Applied Physics Letters, Vol. 96, No. 2, p. 021902, 2010.

[5] A. Nagoya, R. Asahi, R. Wahl, and G. Kresse, "Defect formation and phase stability of Cu_2ZnSnS_4 photovoltaic material," Physical Review B, Vol. 81, p. 113202, 2010.

[6] S. Rahaman, M. A. Sunil, M. K. Singha, K. Ghosh, "Optimization and fabrication of low cost Cu_2SnS_3/ZnS thin film heterojunction solar cell using ultrasonic spray pyrolysis," Optical Materials, Vol. 124, p. 111838, 2022.

[7] D. Tiwari, T. K. Chaudhuri, T. Shripathi, U. Deshpande, R. Rawat, "Non-toxic, earth-abundant 2% efficient Cu_2SnS_3 solar cell based on tetragonal films direct-coated from single metal-organic precursor solution," Solar Energy Materials and Solar Cells, Vol. 113, pp. 165–170, 2013.

[8] M. Y. Alia, M. A. Abedin, M. S. Hossain, and E. S. Hossain, "Optimization of monoclinic Cu_2SnS_3 (CTS) thin film solar cell performances through numerical analysis," Chalcogenide Letters, Vol. 17, No. 2, pp. 85–98, 2020.

[9] J. Han, Y. Zhou, Y. Tian, Z. Huang, X. Wang, J. Zhong, Z. Xia, B. Yang, H. Song, and J. Tang, "Hydrazine processed Cu_2SnS_3 thin film and their application for photovoltaic devices," Frontiers in Optoelectronics, Vol. 7, pp. 37–45, 2014.

[10] D. M. Berg, R. Djemour, L. Gütay, G. Zoppi, S. Siebentritt, P. J. Dale, "Thin film solar cells based on the ternary compound Cu_2SnS_3," Thin Solid Films, Vol. 520, No. 19, pp. 6291–6294, 2012.

[11] J. Chantana, K. Tai, H. Hayashi, T. Nishimura, Y. Kawano, and T. Minemoto, "Investigation of carrier recombination of Na-doped Cu_2SnS_3 solar cell for its improved conversion efficiency of 5.1%," Solar Energy Materials and Solar Cells, Vol. 206, p. 110261, 2020.

[12] A. C. Lokhande, R. B. V. Chalapathy, M. He, E. Jo, M. Gang, S. A. Pawar, C. D. Lokhande, and J. H. Kim, "Development of Cu_2SnS_3(CTS) thin film solar cells by physical techniques: a status review," Solar Energy Materials and Solar Cells, Vol. 153, pp. 84–107, 2016.

[13] M. Bouaziz, M. Amlouk, and S. Belgacem, "Structural and optical properties of Cu_2SnS_3 sprayed thin films," Thin Solid Films, Vol. 517, No. 7, pp. 2527–2530, 2009.

[14] S. Rahaman, M. A. Sunil, M. K. Singha, K. Ghosh, "Studies of ultrasonically sprayed Cu_2SnS_3 thin Films by varying Sn concentration," Materials Today Proceedings, Vol. 43, part 6, pp. 3938–3941, 2021.

[15] N. Akcay, V. F. Gremenok, Y. Ozen, K. P. Buskis, E. P. Zaretskaya, S. Ozcelik, "Investigation on photovoltaic performance of Cu_2SnS_3 thin film solar cells fabricated by RF-sputtered In_2S_3 buffer layer," Journal of Alloys and Compounds, Vol. 949, p. 169874, 2023.

[16] V. V. Kutwade, K. P. Gattu, M. E. Sonawane, D. A. Tonpe, I. M. S. Mohammed, R. Sharma, "Theoretical modeling and optimization: Cd-free CTS/Zn(O,S)/ZnO thin film solar cell," Materials Today Communications, Vol. 29, p. 102972, 2021.

[17] M. Y. Zaki, F. Sava, I. D. Simandan, A. T. Buruiana, C. Mihai, A. Velea, and A. C. Galca, "Effect of the stacking order, annealing temperature and atmosphere on crystal phase and optical properties of Cu_2SnS_3," Scientific Reports, Vol. 12, p. 7958, 2022.

[18] M. T. Islam, A. Kumar, and A. K. Thakur, "Defect density control using an intrinsic layer to enhance conversion efficiency in an optimized SnS solar cell," Journal of Electronic Materials, Vol. 50, pp. 3603–3613, 2021.

[19] AMPS Manual, The Electronic Materials and Processing Research Laboratory, Pennsylvania State University, 2007.

[20] M. A. A. Noman, S. Siraj, M. J. Abden, N. Amin, and M. A. Islam, "A numerical analysis of BSF layers for ultra-thin high efficiency CdTe thin film solar cell," Chalcogenide Letters, Vol. 16, No. 4, pp. 185–193, 2019.

[21] E. Puente-López and M. Pal, "Numerical simulation and optimization of physical properties for high efficiency $CuSbS_2$ thin film solar cells," Optik - International Journal for Light and Electron Optics, Vol. 272, 170233, 2023.

[22] M. Burgelman, J. Verschraegen, S. Degrave, and P. Nollet, "Modeling thin film PV devices," Progress in Photovoltaics: Research and Applications, Vol. 12, pp. 143–153, 2004.

[23] Y. Wei, Z. Ma, X. Zhao, J. Yin, Y. Wu, L. Zhang, and M. Zhao, "Improving the performance of $Cu_2ZnSn(S,Se)_4$ thin film solar cells by SCAPS simulation," Materials Science and Engineering: B, Vol. 303, p. 117296, 2024.

[24] M. S. Hossain, N. Amin, and T. Razykov, "Prospects of back contacts with back surface fields in high efficiency ZnxCd1−xS/CdTe solar cells from numerical modeling," Chalcogenide Letters, Vol. 8, No. 3, pp. 187–198, 2011.

[25] O. M. Hussain, P. S. Reddy, B. S. Naidu, S. Uthanna, and P. J. Reddy, "Characterization of thin film ZnCdS/CdTe solar cells," Semiconductor Science and Technology, Vol. 6, pp. 690–694, 1991.

[26] M. S. Hossain, N. Amin, M. A. Matin, M. M. Aliyu, T. Razykov, and K. Sopian, "A numerical study on the prospects of high efficiency ultra-thin $Zn_xCd_{1-x}S$/CdTe solar cell," Chalcogenide Letters, Vol. 8, No. 3, pp. 263–272, 2011.